JurnalPolimesin
Department of Mechanical Engineering
State Polytechnic of Lhokseumawe
http://e-jurnal.pnl.ac.id/polimesin
e-ISSN : 2549-1199 No. : 2 Month : April
p-ISSN : 1693-5462 Volume : 23 Year : 2025

Processing dates: received on 2024-12-16, reviewed on 2025-01-17, accepted on 2025-02-24 and online avaibility on 2042-04-01

Numerical simulation of the effect of synthetic jet actuators on aerodynamic performance in high-lift device configurations

Mohamad Yamin*, Kukuh Ivan Apriyadi, Riyan Firmansyah
Department of Mechanical Engineering, University of Gunadarma, Depok 16424, Indonesia
*Corresponding author: mohay@staff.gunadarma.ac.id

Abstract

The aviation industry faces significant challenges in reducing environmental impacts, particularly fuel consumption and noise pollution. To address these issues, various aerodynamic optimization and flow control technologies have been developed to enhance aircraft efficiency. One promising approach is Active Flow Control (AFC), particularly in wing-flap configurations. However, cambered flaps can induce flow separation, leading to increased drag and reduced aerodynamic performance. This study investigates the application of AFC using Zero Net Mass Flux (ZNMF) to mitigate flow separation and improve aerodynamic efficiency. Numerical simulations were conducted using ANSYS Fluent, employing the Delayed Detached Eddy Simulation –Spalart-Allmaras (DDES-SA) turbulence model to accurately capture flow separation and vortex structures. The research explores a novel ZNMF geometry, analyzing different frequency and velocity parameters to determine the optimal settings for suppressing flow separation. The results demonstrate that the Synthetic Jet Actuator (SJA) significantly enhances aerodynamic efficiency by optimizing the C_L/C_D ratio through drag reduction without major lift loss. Optimal performance is achieved at frequencies of 150–300 Hz and jet velocities of ≥150 m/s, stabilizing airflow, reducing flow separation, and suppressing vortex formation. At an AOA of 0°, a frequency of 100 Hz provides the greatest CL reduction, while at an AOA of 10°, frequencies of 100–250 Hz substantially improve the C_L/C_D ratio. This study confirms that SJA is an effective strategy for drag reduction and aerodynamic optimization. These findings highlight its potential to improve aircraft performance, reduce fuel consumption and CO_2 emissions, and contribute to more sustainable aviation technology

Keywords:
Active flow control, zero-net-mass-flux, high lift device, CFD, aerodynamics.

1 Introduction

The aviation industry is actively working to reduce its environmental impact by focusing on carbon dioxide emissions, noise pollution, and fossil fuel consumption. To achieve this, various technologies and strategies have been developed, including improving aircraft aerodynamic efficiency and applying more environmentally friendly energy sources [1]. One of the main approaches is the development of Active Flow Control (AFC) systems aimed at reducing flow separation and drag on aircraft wings, thereby improving fuel efficiency and reducing the environmental impact [2]. Various flow separation control strategies, such as Boundary Layer Control (BLC) through blowing and suction, aim to delay or prevent flow separation and enhance the aerodynamic characteristics of airfoils, such as NACA 0021 [3]. Other techniques, such as Pulsed Jet Actuators (PJA), use fluid oscillators to enhance the boundary layer momentum without moving parts and have significant potential for industrial applications [4]. Synthetic Jet Actuators (SJAs) have been proven effective in enhancing aerodynamic performance by manipulating airflow without adding mass. This technology works by periodically expelling and ingesting fluid through holes on the airfoil surface, creating vortices that affect the surrounding airflow, potentially increasing the lift and reducing the drag. The application of SJAs to different airfoil designs yielded significant results. The use of Dual Synthetic Jet Actuators (DSJA) on an optimized NACA 0012 airfoil increased the lift-to-drag ratio by 13.5% at high angles of attack. This improvement was achieved through the Coanda effect, which manipulates the flow field and enhances lift [5]. On the NACA 0025 airfoil, the use of MEMS-based synthetic jets reduced flow separation, increased lift by up to 2.5 times, and reduced drag by 50% compared with conditions without flow control [6]. SJAs are also effective in delaying flow separation on symmetric airfoils, which is beneficial at high angles of attack. In post-stall conditions, the use of SJAs at the leading edge of the NACA 0015 airfoil energizes the boundary layer, delays flow separation, and enhance lift, even at high angles of attack [7]. The use of SJAs on airfoils with circulation control, such as NACA 0015, has shown optimal lift enhancement at certain excitation frequencies, reinforcing the potential of this technology to improve the aerodynamic performance of airfoils under various operational conditions [8]. Additionally, synthetic jets can mimic the effect of leading-edge tubercles, providing a biomimetic approach to improve aerodynamic characteristics under both pre-stall and post-stall conditions [7].

In recent years, the use of Zero Net Mass Flux (ZNMF) devices as AFC has made significant progress in its application to airfoils, similar to piezo-actuators embedded in wing flap systems [9]. Seifert and Pack were the first to conduct AFC experiments on the NACA 0015 airfoil at high Reynolds numbers [10]. On the other hand, many researchers have used numerical methods to examine the impact of ZNMF synthetic jets on various airfoils [11], [12], [13]. Numerical simulations using the Unsteady Reynolds-Averaged Navier-Stokes (URANS) and Large Eddy Simulation (LES) methods were employed to optimize the actuation parameters of the ZNMF on high-lift airfoils. URANS simulations help predict aerodynamic performance improvements by optimizing the gap geometry and ZNMF placement, as applied to the Deutsches Zentrum für Luft- und Raumfahrt (DLR) F15 Leading-Edge Extension (LLE) (DLR-F15LLE) airfoil [14]. Meanwhile, three-dimensional LES simulations provide deep insights into the effects of ZNMF jets on the flow separation, flow dynamics, and control effectiveness of the NACA 0015 airfoil [15]. This actuator utilizes a piston mechanism to generate a synchronized jet flow through blowing and suction at the airfoil's leading edge. This method has been proven to prevent stall at high angles of attack by maintaining attached flow over the airfoil surface, especially at high excitation frequencies [16]. ZNMF jets create vortices through alternating blowing and suction, injecting momentum into the boundary layer without adding mass. This process can generate coherent vortex structures that influence the flow field around the aerodynamic surface [17]. The optimization of actuation parameters, such as actuation frequency, is also an important factor in improving lift and controlling flow separation, where stability analysis and numerical simulations help identify the optimal frequency for effective flow control [18]. Numerical simulations using the URANS model have shown that ZNMF jets can force flow reattachment, resulting in a 30% reduction in boundary layer thickness and a 17.6% increase in lift-to-drag ratio [12]. Marouf et al. [9] demonstrated that ZNMF devices can cause flow reattachment and delay flow separation in wings with flaps. Steady blowing with different jet intensities enhances flow reattachment, with the spacing between the jets forming two opposing vortices that interact with each other. The ZNMF is the most effective upstream of the flow separation to avoid jet momentum loss.

This study explored a new ZNMF geometry position that was not previously evaluated. By examining various parameters, such as frequency and jet velocity, this research aims to find the most efficient parameter settings to address flow separation and improve aircraft aerodynamic efficiency. The advantage of this study lies in the utilization of an innovative ZNMF geometry configuration, building upon previous research, which is expected to provide a more effective and practical solution for enhancing aircraft aerodynamic performance.

2 Numerical simulation method

2.1 Description of the studied case

This study investigated the impact of the ZNMF position on drag reduction on an A320 aircraft wing using an NACA 23015 airfoil. This airfoil has a span length of 0.27 m and a chord length of 1 m, with the ZNMF installed on a flap with a chord size of 0.35 m. The SJA holes used were 10 mm in diameter and were positioned, as shown in Fig. 1. The model was evaluated using ANSYS Fluent 2023 R1 Academic Licence Software at various angles of attack. Directed jets were introduced as an additional innovation to enhance the performance of flow control systems [11].

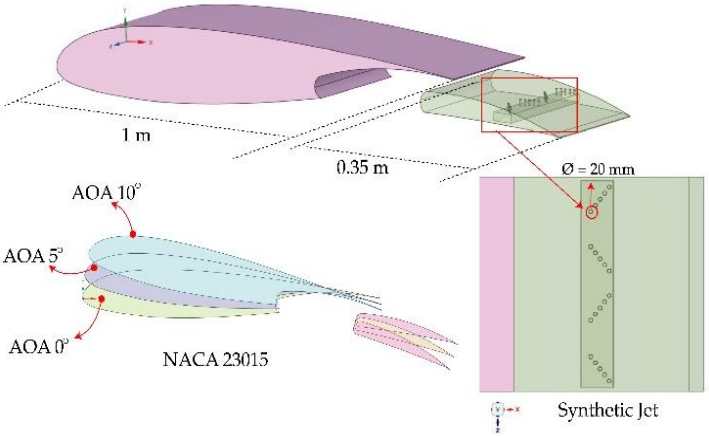

Fig. 1. Geometry model

2.2 Governing equations and turbulence model

In this study, the fluid flow was analyzed using the Navier-Stokes equations, which include the conservation of mass and momentum laws [19]. The Continuity Equation, which states that the mass of the fluid remains constant throughout the flow, can be seen in Eq. (1).

$$\frac{\partial uj}{\partial xj} = 0 \tag{1}$$

Next, the momentum equation as shown in Eq. (2) is used to describe the changes in the velocity and pressure of the fluid.

$$\frac{\partial ui}{\partial t} + \frac{\partial}{\partial xj}(u_j u_i) = -\frac{\partial}{\partial x_i}\left(\frac{p}{\rho_0}\right) + \frac{\partial}{\partial x_j}\left[v_m\left(\frac{\partial u_i}{\partial x_j} + \frac{\partial u_j}{\partial x_i}\right) - \frac{2}{3}v_m\frac{\partial u_k}{\partial x_k}\delta_{ij}\right] \tag{2}$$

where u is the fluid velocity, p is the fluid pressure, ρ is the fluid density, μ is the fluid viscosity, and x represents the spatial coordinates. Because the flow velocity is much lower than the speed of sound (Mach < 0.3), the assumption of an incompressible fluid was applied. Therefore, terms related to compressibility can be neglected (Eq. (3)).

$$-\frac{2}{3}\frac{\partial u_k}{\partial x_k}\delta_{ij} = 0 \tag{3}$$

However, this term is included to maintain the stability of the solution during numerical computation. The turbulence model used in this CFD approach was the Detached Eddy Simulation (DES) model, which was first introduced by Shur et al. [20]. This model combines the Reynolds-averaged Navier–Stokes (RANS) method and LES to improve the accuracy of turbulent flow simulations [21], [22]. In this approach, the Spalart-Allmaras turbulence model is used to predict the near-wall (boundary layer) flow using the RANS method and to model the flow far from the wall using the LES method [23]. Delayed Detached Eddy Simulation - Spalart Allmaras (DDES-SA) was chosen as it combines RANS (near-wall) and LES (off-wall), improving turbulent flow accuracy with computational efficiency.

2.3 Computational domain, mesh setup, and boundary conditions

The computational domain measures (4.5m x 3m x 3m) with the inlet velocity defining the flow entering the domain, providing realistic initial conditions for the simulation [24]. The use of symmetry helps reduce the computational load by simulating only a portion of the domain, which is effective if the flow is expected to be uniform on both sides [25]. Meanwhile, the outlet pressure condition ensures smooth flow out of the domain, preventing backflow, and maintaining the stability of the simulation, which is crucial for convergence to accurate results [26]. This is divided into inlet jet velocity, wall jet, and outlet jet pressure, as shown in Fig. 2.

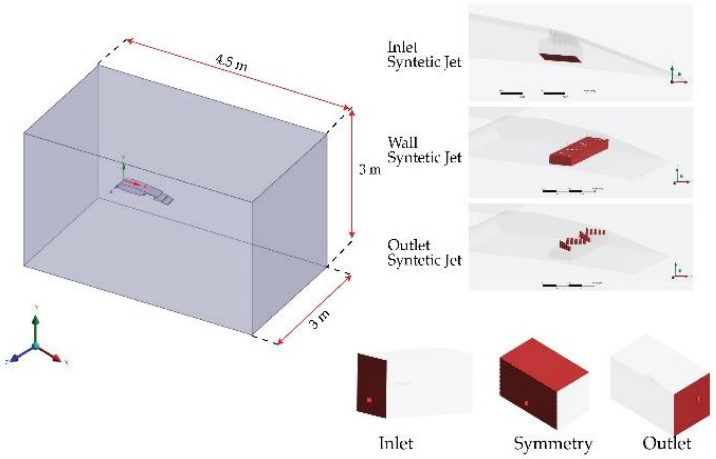

Fig. 2. Computational domain

The meshing in CFD divides the physical domain into small elements to numerically solve the fluid flow equations [27], as shown in Fig. 3. Grid validation was performed for four variations: coarse, medium, fine, and very fine, as indicated in Table 1. Meshing uses Ansys Meshing with a flexible tetrahedral method for irregular shapes [28], [29].

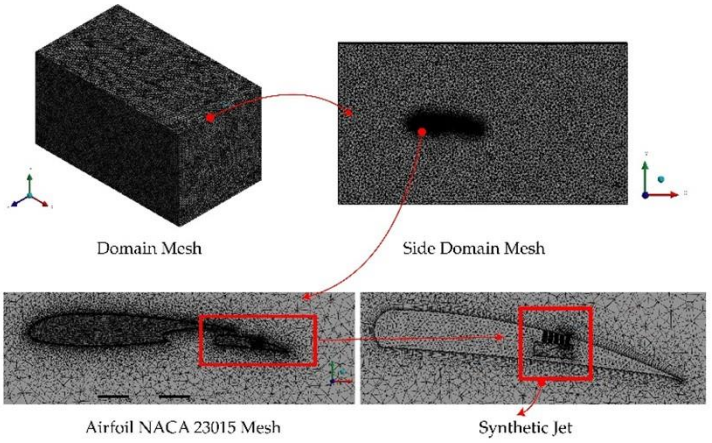

Fig. 3. Meshing

The patch-conforming algorithm ensures that the mesh conforms to the geometry, which is important for accurate simulations, especially in fluid dynamics applications, where the mesh quality influences the accuracy of the results [30]. Face meshing with an element size of 4 mm and local mesh of 0.5 mm was applied to critical areas, such as the leading and trailing edges of the airfoil, to capture the flow

gradients and flow separation phenomena accurately. Body sizing with an element size of 75 mm was applied to the fluid domain to reduce the number of elements in areas with small flow gradients, thereby saving computational resources. The simulation can capture turbulent flow in detail without compromising computational efficiency with a total of three million mesh elements (fine mesh). The selection of appropriate element sizes in different areas enhances the accuracy of the simulation results and optimizes resource usage.

Table 1. Performance comparison with and without SJA at 0° AOA for different element sizes

Configuration	Type	Coarse	Medium	Fine	Very Fine
Without SJA	Element	1001473	2250265	3105961	4540802
	C_L	0.047	0.048	0.048	0.049
	C_D	0.020	0.020	0.021	0.020
With SJA	Element	1656990	2902621	3782715	5230029
	C_L	0.036	0.037	0.035	0.037
	C_D	0.018	0.017	0.017	0.018

This simulation used the DDES-SA model with vorticity-based production and delayed DES. The air fluid has a 1.225 kg/m³ density, viscosity 1.7894×10^{-5} kg/ms, and an inlet velocity of 68 m/s. The turbulence conditions were set with a turbulence intensity of 5%, reflecting the ratio of fluctuating velocity to average flow velocity. In comparison, the ratio of turbulent viscosity to dynamic viscosity was set to 10% to indicate a high level of mixing. The solver uses a pressure-based approach in transient conditions with the SIMPLE scheme for pressure-velocity coupling, least square cell-based discretization for gradients, second-order upwind for pressure, and Bounded Central Differencing for momentum. The transient formulation uses a bounded second-order implicit. The relaxation parameters included momentum (0.7), pressure (0.3), and modified turbulent viscosity (0.8), with the residual monitor set to 10^{-3} to ensure stability and convergence, as shown in Table 3. As shown in Table 2, the variation in jet velocity ranges from 70 to 300 m/s with a frequency of 50-250 Hz.

Table 2. Variation in inlet velocity, jet velocity, and frequency

Case	U_∞ [m/s]	V_{jet} [m/s]	Frequency [Hz]
1	68	70, 100, 150, 200	50
2			100
3			150
4			200
5			250
6			300

Table 3. Solver configuration and numerical settings in CFD simulation

General Setting		Explicit relaxation factors	
Solver	Pressure-Based	Momentum	0.7
Time	Transient	Pressure	0.3
Velocity formulation	Absolute	Under-relaxation factors	
Solution methods		Density	1
Pressure-Velocity Coupling	Simple scheme	Body forces	1
Spacial discretization Gradients	Least Square Cell-Based	Modified Turbulent Viscosity	0.8
Pressure	Second Order Upwind	Turbulent viscosity	1
Momentum	Bounded Central Differencing	Residual monitors	
Modified Turbulent Viscosity	First Order Upwind	Continuity equation	10^{-3}
BCD Scheme Boundedness	1	X-velocity component	10^{-3}
Transient Formulation	Bounded Second Order Implicit	Y, Z-velocity components	10^{-3}
Time step size [s]	$\frac{1}{\frac{f}{360}}$	k, ω	10^{-3}

This range was selected to accurately model the turbulent flow applied to the airfoil's upper surface [9]. Since the synthetic jet velocity cannot be directly set as a time-dependent function in Fluent because Boundary Conditions (BC) only support constant valuesa C-based User Defined Function (UDF) is required. This UDF implements velocity as a sinusoidal function, allowing for periodic jet behavior. The jet frequency is defined using the sinusoidal equation [31], [32] in Eq. (4) and the jet period in Eq. (5).

$$V_{jet}(t) = V_{Max}\sin(\omega t) \tag{4}$$

$$\omega = 2\pi f \tag{5}$$

The UDF is compiled in Fluent™ and then applied to the velocity-inlet boundary condition. The selection of jet frequency and velocity significantly impacts the simulation results, particularly in increasing the lift coefficient (C_L) and reducing the drag coefficient (C_D). The synthetic jet frequency is defined in the UDF using Eq. (5). Where $f = 20\ Hz$ (as per specifications) [33]. The frequency is controlled in Fluent by defining a time-dependent velocity profile using the UDF. The simulation is run in transient mode with a sufficiently small time step to capture the oscillation dynamics accurately. The lift and drag coefficients are calculated using the following equation. To evaluate aerodynamic performance, the (C_L) and (C_D) were calculated using Eqs (6 and 7),

$$C_D = \frac{F_D}{0.5\rho c U_\infty^{\ 2}} \tag{6}$$

$$C_L = \frac{F_L}{0.5\rho c U_\infty^2} \tag{7}$$

2.4 Validation model

Validation was performed by comparing the experimental data and CFD simulations, mainly focusing on the drag and lift coefficients. The experiment was conducted using a wind tunnel with a wing model featuring a NACA 23015 airfoil with a chord length of 165 mm and a span of 300 mm. The airflow was tested at a free-stream velocity of 25 m/s in a subsonic blow-down wind tunnel with a test section size of 600 mm × 600 mm × 2000 mm. This wind tunnel used compressed air from a compressor and had a maximum velocity of 50 m/s with a compression ratio of 9:1. The measured experimental data included the lift and drag forces, which

were then used to calculate the C_D and C_L. The CFD simulation was performed with the same wing model, and the results were compared with the experimental results to validate the accuracy of the CFD model in representing real flow phenomena. A comparison of C_L and C_D values from both the experiments and CFD simulations (Table. 4) was used to evaluate the validity of the simulation and ensure that the simulation results reflect the actual flow conditions in the experiment.

Table 4. Comparison of experimental results and CFD simulation at AOA 0°

Parameter	CFD (Present Study)	Experiment [33]
C_L	0.052	0.056
C_D	0.015	0.010

The geometry model is modified with a chord length of 1 m and a span of 0.27 m, and a flap with a length of 0.35 m and a span of 0.27 m is added. The simulation was performed at a speed of 68 m/s and an AOA of 0°. Additional modifications include using a SJA on the flap with a jet velocity of 70 m/s and frequency (F) of 50 Hz to improve the aerodynamic performance. To ensure the simulation accuracy, validation was conducted through a mesh study with various element sizes to determine the optimal configuration that produces the simulation results, as shown in Fig. 4.

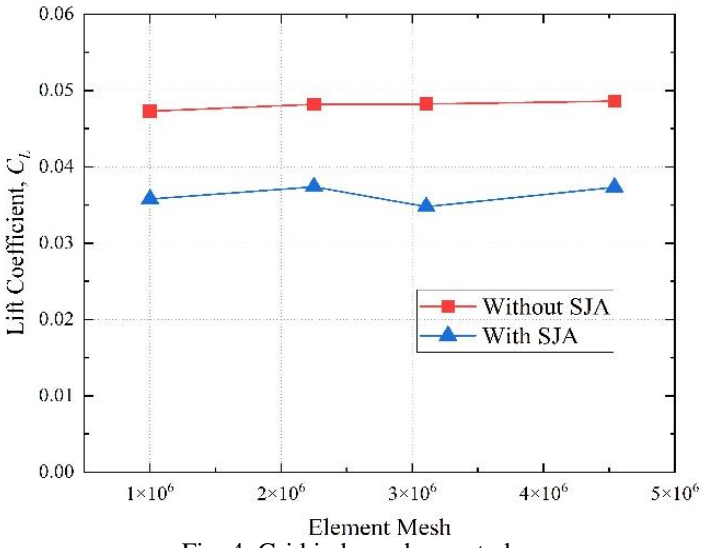

Fig. 4. Grid independence study

3 Results and discussion

This study demonstrates that the synthetic jet plays a role in controlling the C_L of the NACA 23015 airfoil at a flow velocity of 68 m/s. As shown in Fig. 5, at AOA 0°, the activation of the synthetic jet with a velocity of 70 m/s and a frequency range of 50–300 Hz reduces C_L from 0.04822 to 0.03477–0.0378, with the most significant reduction occurring at 100 Hz (C_L = 0.03477). This indicates that the synthetic jet effectively disrupts the airflow and reduces lift force at small angles of attack. At AOA 5°, the decrease in C_L is more limited, ranging from 0.07675 to 0.07791, suggesting a more stable influence. Meanwhile, at AOA 10°, C_L slightly decreases from 0.10699 to 0.09095–0.09196, indicating that the effectiveness of the synthetic jet diminishes at higher angles of attack.

Furthermore, Fig. 6 illustrates that synthetic jet velocity also affects C_L. At AOA 0°, increasing the jet velocity from 70 m/s (C_L = 0.0378) to 200 m/s (C_L = 0.03611) enhances the reduction of C_L. However, at AOA 5° and 10°, variations in jet velocity result in only minor changes, with C_L remaining in the range of 0.07675–0.07791 at AOA 5° and 0.09196–0.09234 at AOA 10°.

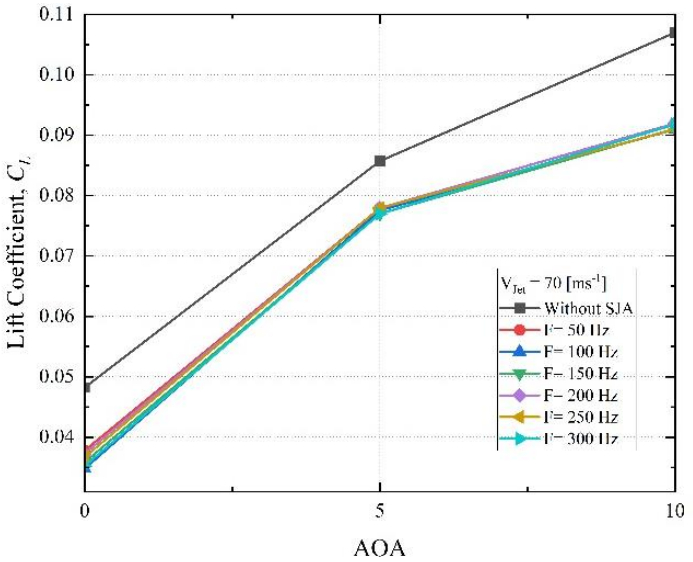

Fig. 5. Effect of SJA frequency on lift coefficient and jet velocity 70 m/s

This consistency suggests that the synthetic jet is more effective in reducing lift force at low AOA, but its impact is limited at moderate to high angles of attack. The synthetic jet is most effective in controlling airflow at low AOA, particularly in preventing flow separation. However, at higher angles of attack, its influence becomes increasingly restricted, regardless of frequency or jet velocity variations. Therefore, the optimization of synthetic jet implementation should consider the interaction of aerodynamic parameters to enhance airfoil performance under various operating conditions.

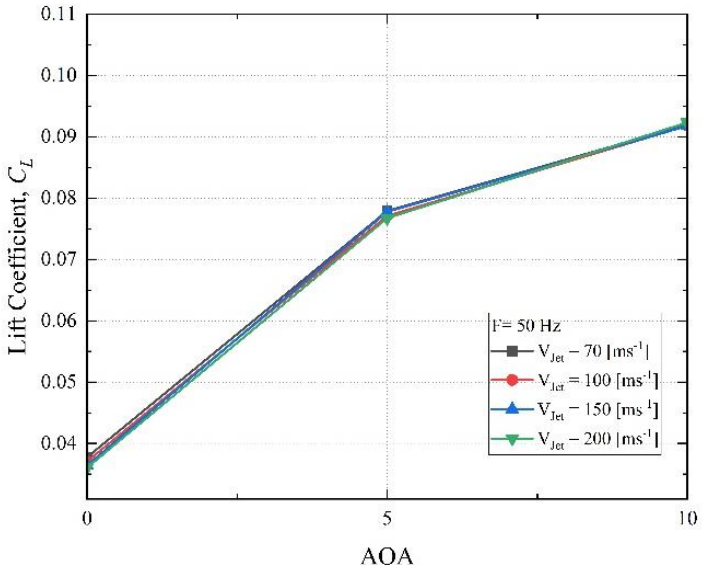

Fig. 6. Effect of jet velocity on drag coefficient at 50 Hz frequency and U_∞=68 m/s

The analysis of the lift-to-drag ratio (C_L/C_D) at AOA 0° and 10° indicates that the effectiveness of the SJAvaries depending on the frequency (F) and jet velocity (V_{jet}). Based on Fig. 7, at AOA 0°, C_L/C_D decreases at lower frequencies (50–100 Hz) compared to the condition without SJA. This effect is particularly noticeable at V_{jet} = 70 m/s, suggesting that SJA activation at low frequencies tends to increase drag without significantly enhancing lift. However, at higher frequencies (150–300 Hz), C_L/C_D begins to increase, particularly at $V_{jet} \geq$ 150 m/s, with the highest value observed at F = 150 Hz and v_jet = 200 m/s (C_L/C_D = 2.14647). This indicates that at AOA 0°, the effectiveness of SJA in improving aerodynamic efficiency is more optimal at moderate to high frequencies with high jet velocity.

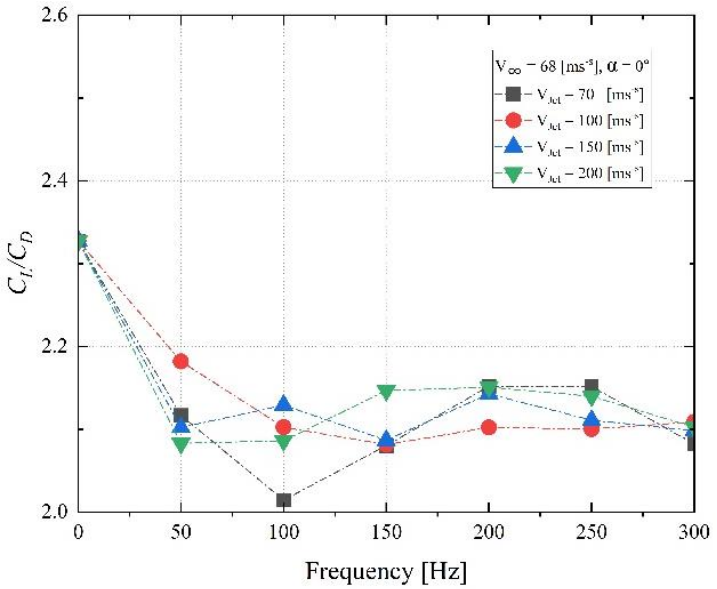

Fig. 7. Effect of SJA on C_L/C_D at AOA 0°

Meanwhile, Fig. 8 shows that at AOA 10°, SJA usage increases C_L/C_D compared to the condition without SJA, particularly at moderate to high frequencies (100–250 Hz) and higher jet velocities. The highest C_L/C_D increase occurs at F = 100 Hz and V_{jet} = 70 m/s (C_L/C_D = 2.5264), indicating that at a higher angle of attack, SJA can help improve aerodynamic efficiency by modifying the airflow around the airfoil.

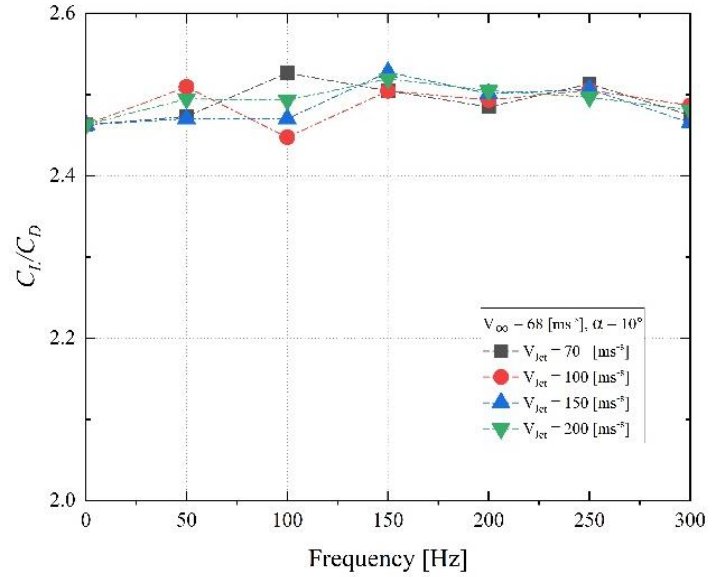

Fig. 8. Effect of SJA on C_L/C_D at AOA 10°

When correlated with Fig. 5, which presents the C_L, it is evident that at AOA 10°, SJA activation causes only a minor decrease in C_L, meaning that *variations more influence C_L/C_D change*s in drag. On the other hand, Fig. 6, which illustrates the effect of jet velocity on C_L, shows that variations in V_{jet} have a smaller impact on C_L at higher angles of attack. Consequently, the increase in C_L/C_D at AOA 10° is primarily attributed to drag reduction rather than lift enhancement.

Overall, these findings suggest that SJA is more effective in enhancing aerodynamic efficiency (C_L/C_D) at a higher AOA (10°) compared to AOA 0°, especially at moderate to high frequencies (100–250 Hz) and jet velocities (≥150 m/s). At AOA 0°, the effect of SJA on C_L/C_D is more variable, with low frequencies tending to reduce aerodynamic efficiency due to increased drag. In contrast, higher frequencies can slightly improve C_L/C_D by reducing aerodynamic resistance.

The relationship between the C_L/C_D analysis results and the C_L can be explained by examining how the SJA influences airflow around the airfoil, directly impacting C_L and C_D. As shown in Fig. 5, activating the SJA at AOA 10° causes a relatively small decrease in C_L, indicating that CD influences the primary changes in the CL/CD ratio more than C_L. Fig. 9 (Velocity Contour) illustrates that the SJA helps create a more uniform velocity distribution around the airfoil, contributing to sgreater flow stability and reducing flow separation.

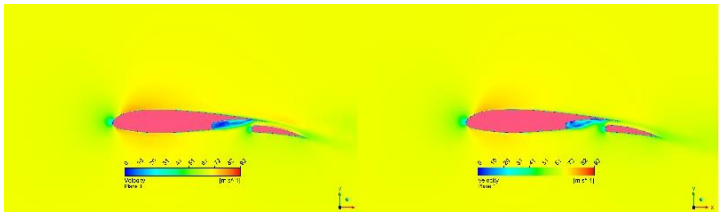

(a) (b)

Fig. 9. Velocity contour (a) without SJA (b) with SJA

This reduction in separation prevents a significant decrease in C_L, especially at medium to high frequencies (150–300 Hz) and high jet velocities (≥150 m/s). Thus, although the SJA does not significantly increase C_L, the improved flow stability helps maintain a relatively constant lift force. Furthermore, Fig. 10 (Streamline Contour) demonstrates that the airflow is more organized with SJA activation.

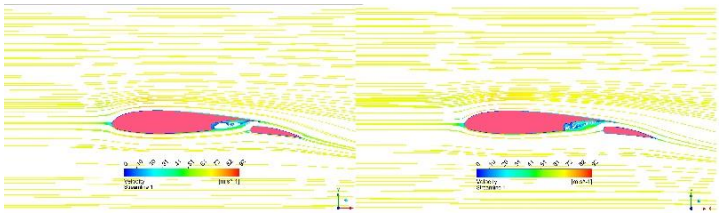

(a) (b)

Fig. 10. Streamline contour (a) without SJA (b) with SJA

In the baseline condition, the flow exhibits disturbances and sharp turns, which can lead to flow separation and a reduction in C_L. The SJA minimizes flow separation, allowing C_L to remain more stable, particularly at higher jet velocities. Additionally, Fig. 11 (Vortex Contour) reveals that the SJA significantly reduces vortex formation, directly contributing to C_D reduction.

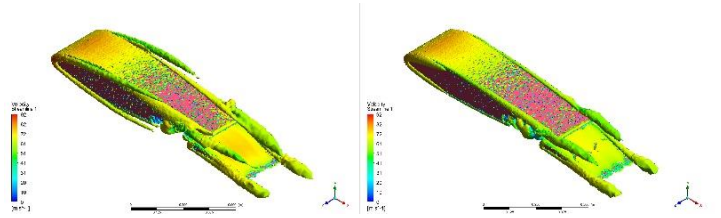

(a) (b)

Fig. 11. Vortex contour (a) without SJA (b) with SJA

In the baseline condition, strong vortices behind the airfoil increase drag, reducing C_L/C_D. However, with SJA activation at V = 70 m/s and F = 300 Hz, vortex formation is significantly reduced, leading to a decrease in C_D without causing a significant change in C_L. From this analysis, it can be concluded that the SJA is more effective in reducing drag than increasing lift. Therefore, the improvement in C_L/C_D observed in Fig.s 7 and 8 is primarily due to a more effective reduction in C_D rather than an increase in C_L. The combination of medium to high frequencies (150–300 Hz) and high jet velocities (≥150 m/s) demonstrates the optimal effectiveness of the SJA in enhancing aerodynamic efficiency without significantly compromising C_L.

4 Conclusions

The aviation industry faces significant challenges in reducing environmental impacts, particularly fuel consumption and noise pollution. To address these issues, various aerodynamic optimization and flow control technologies have been developed to enhance aircraft efficiency. One promising approach is AFC, particularly in wing-flap configurations. However, cambered flaps can induce flow separation, leading to increased drag and reduced aerodynamic performance.

This study investigates the application of AFC using ZNMF to mitigate flow separation and improve aerodynamic efficiency. Numerical simulations were conducted using ANSYS Fluent, employing the DDES-SA turbulence model to accurately capture flow separation and vortex structures. The research explores a novel ZNMF geometry, analyzing different frequency and velocity parameters to determine the optimal settings for suppressing flow separation.

The results demonstrate that the Synthetic Jet Actuator (SJA) significantly enhances aerodynamic efficiency by optimizing the C_l/C_d ratio through drag reduction without major lift loss. Optimal performance is achieved at frequencies of 150–300 Hz and jet velocities of ≥150 m/s, stabilizing airflow, reducing flow separation, and suppressing vortex formation. At an AOA of 0°, a frequency of 100 Hz provides the greatest CL reduction, while at an AOA of 10°, frequencies of 100–250 Hz substantially improve the C_l/C_d ratio. This study confirms that SJA is an effective strategy for drag reduction and aerodynamic optimization. These findings highlight its potential to improve aircraft performance, reduce fuel consumption and CO_2 emissions, and contribute to more sustainable aviation technology.

References

[1] A. Bravo, D. Vieira, and G. Ferrer, "Emissions of future conventional aircraft adopting evolutionary technologies," *Journal of Cleaner Production*, vol. 347, p. 131246, May 2022, doi: 10.1016/j.jclepro.2022.131246.

[2] A. Shmilovich, Y. Yadlin, P. M. Vijgen, and R. Woszidlo, "Applications of flow control to wing high-lift leading edge devices on a commercial aircraft," in *AIAA SCITECH 2023 Forum*, in AIAA SciTech Forum. , American Institute of Aeronautics and Astronautics, 2023. doi: 10.2514/6.2023-0656.

[3] J. S. M. Ali, M. F. Amran, and N. A. Mohamad, "Experimental study on the effect of boundary layer control on the aerodynamics characteristics of NACA 0021 aerofoil," *Journal of Advanced Research in Fluid Mechanics and Thermal Sciences*, vol. 94, no. 1, Art. no. 1, Apr. 2022, doi: 10.37934/arfmts.94.1.129137.

[4] S. Löffler, C. Ebert, and J. Weiss, "Fluidic-oscillator-based pulsed jet actuators for flow separation control," *Fluids*, vol. 6, no. 4, Art. no. 4, Apr. 2021, doi: 10.3390/fluids6040166.

[5] R. Srinath, R. Mukesh, I. Hasan, and P. R. Krishnan, "CFD Investigation of Dual Synthetic Jets on an Optimized Aerofoil's Trailing Edge," *Journal of Applied Fluid Mechanics*, vol. 17, no. 11, pp. 2448–2464, Sep. 2024, doi: 10.47176/jafm.17.11.2709.

[6] K. Xu, P. Lavoie, and P. Sullivan, "Separation control on an naca 0025 airfoil using an array of MEMS-based synthetic jets," presented at the ASME 2022 Fluids Engineering Division Summer Meeting, American Society of Mechanical Engineers Digital Collection, Sep. 2022. doi: 10.1115/FEDSM2022-87621.

[7] L. Wang, Z. Li, and L. Feng, "Improvement of poststall performance of NACA 0015 airfoil using leading-edge synthetic jet array," *Journal of Aerospace Engineering*, vol. 37, no. 2, p. 04023116, Mar. 2024, doi: 10.1061/JAEEEZ.ASENG-5243.

[8] P. Itsariyapinyo and R. N. Sharma, "Experimental study of a NACA0015 circulation control airfoil using synthetic jet actuation," *AIAA Journal*, vol. 60, no. 3, pp. 1612–1629, 2022, doi: 10.2514/1.J060508.

[9] A. Marouf *et al.*, "Unsteady CFD simulations for active flow control," in *AIAA AVIATION 2021 FORUM*, in AIAA AVIATION Forum. , American Institute of Aeronautics and Astronautics, 2021. doi: 10.2514/6.2021-2854.

[10] A. Seifert and L. G. Pack, "Oscillatory control of separation at high Reynolds numbers," *AIAA Journal*, vol. 37, no. 9, pp. 1062–1071, 1999, doi: 10.2514/2.834.

[11] A. Marouf *et al.*, "CFD simulations of active flow control devices applied on a cambered flap," in *AIAA SCITECH 2022 Forum*, American Institute of Aeronautics and Astronautics, 2021. doi: 10.2514/6.2022-1545.

[12] H. Truong, A. Marouf, A. Gehri, J. Vos, M. Braza, and Y. Hoarau, "Numerical investigation of active flow control using zero-net-mass-flux jets around a high-lift morphing cambered wing-flap system," *International Journal of Numerical Methods for Heat & Fluid Flow*, vol. 33, no. 4, pp. 1475–1488, Jan. 2023, doi: 10.1108/HFF-09-2022-0558.

[13] W. Wu, C. Meneveau, R. Mittal, A. Padovan, C. W. Rowley, and L. Cattafesta, "Response of a turbulent separation bubble to zero-net-mass-flux jet perturbations," *Phys. Rev. Fluids*, vol. 7, no. 8, p. 084601, Aug. 2022, doi: 10.1103/PhysRevFluids.7.084601.

[14] R. Montalà, O. Lehmkuhl, and I. Rodriguez, "Large eddy simulations (LES) of a three-element high-lift wing: Exploring the active flow control (AFC) capabilities," *Procedia Computer Science*, vol. 240, pp. 31–41, Jan. 2024, doi: 10.1016/j.procs.2024.07.006.

[15] L. Wang, W. K. Anderson, E. J. Nielsen, P. S. Iyer, and B. Diskin, "Wall-modeled large-eddy simulation method for unstructured-grid navier–stokes solvers," *Journal of Aircraft*, vol. 61, no. 6, pp. 1735–1760, Nov. 2024, doi: 10.2514/1.C037847.

[16] F. Sonkaya, S. Cadirci, and D. Erdem, "Flow separation control on NACA0015 airfoil using synchronized jet actuator," *Journal of Applied Fluid Mechanics*, vol. 15, no. 2, pp. 427–440, Jan. 2022, doi: 10.47176/jafm.15.02.33068.

[17] N. A. Buchmann, C. Atkinson, and J. Soria, "Influence of ZNMF jet flow control on the spatio-temporal flow structure over a NACA-0015 airfoil," *Exp Fluids*, vol. 54, no. 3, p. 1485, Feb. 2013, doi: 10.1007/s00348-013-1485-7.

[18] V. Kitsios, R. Kotapati, R. Mittal, A. Ooi, J. Soria, and D. You, "Numerical simulation of lift enhancement on a NACA 0015 airfoil using ZNMF jets," 2006.

[19] D. S. Weaver and S. Mišković, "A study of RANS turbulence models in fully turbulent jets: a perspective for cfd-dem simulations," *fluids*, vol. 6, no. 8, Art. no. 8, Aug. 2021, doi: 10.3390/fluids6080271.

[20] M. Shur, P. R. Spalart, M. Strelets, and A. Travin, "Detached-eddy simulation of an airfoil at high angle of attack," in *Engineering Turbulence Modelling and Experiments 4*, W. Rodi and D. Laurence, Eds., Oxford: Elsevier Science Ltd, 1999, pp. 669–678. doi: 10.1016/B978-008043328-8/50064-3.

[21] A. K. Jaiswal, A. Bhattacharya, and A. Dewan, "Development of a two-way coupled hybrid RANS- scheme for numerical simulation of turbulent fluid flows," in *Fluid Mechanics and Fluid Power (Vol. 2)*, S. Bhattacharyya and A. C. Benim, Eds., Singapore: Springer Nature, 2023, pp. 71–76. doi: 10.1007/978-981-19-6970-6_14.

[22] G. Kumar, A. De, and H. Gopalan, "Investigation of flow structures in a turbulent separating flow using hybrid RANS-LES model," *International Journal of Numerical Methods for Heat & Fluid Flow*, vol. 27, no. 7, pp. 1430–1450, Jul. 2017, doi: 10.1108/HFF-03-2016-0134.

[23] D. Martins, J. Correia, and A. Silva, “The influence of front wing pressure distribution on wheel wake aerodynamics of an F1 car,” *Energies*, vol. 14, no. 15, Art. no. 15, Jan. 2021, doi: 10.3390/en14154421.
[24] H. S. Abd, A. R. Abdulmunem, and M. H. Jabal, “Numerical investigation of mixture generation due to different inlet and outlet positions,” *International Journal of Low-Carbon Technologies*, vol. 15, no. 2, pp. 308–317, May 2020, doi: 10.1093/ijlct/ctz076.
[25] V. Papkov, N. Shadymov, and D. Pashchenko, “CFD-modeling of fluid flow in ansys fluent using python-based code for automation of repeating calculations,” *Int. J. Mod. Phys. C*, vol. 34, no. 09, p. 2350114, Sep. 2023, doi: 10.1142/S0129183123501140.
[26] K. Kotrasova and V. Michalcova, “The study of the numerical diffusion in computational calculation,” *MATEC Web Conf.*, vol. 310, p. 00039, 2020, doi: 10.1051/matecconf/202031000039.
[27] M. Yamin, H. A. Nashirudin, and R. Firmansyah, “Fenomena Kontrol aliran secara pasif pada konfigurasi ahmed body menggunakan segitiga kendali,” *AME (Aplikasi Mekanika dan Energi): Jurnal Ilmiah Teknik Mesin*, vol. 10, no. 2, Art. no. 2, Sep. 2024, doi: 10.32832/ame.v10i2.763.
[28] Y. Hu, T. Schneider, B. Wang, D. Zorin, and D. Panozzo, “Fast tetrahedral meshing in the wild,” *ACM Trans. Graph.*, vol. 39, no. 4, p. 117:117:1-117:117:18, Aug. 2020, doi: 10.1145/3386569.3392385.
[29] J. Tu, G.-H. Yeoh, and C. Liu, “Chapter 4 - CFD mesh generation: a practical guideline,” in *Computational Fluid Dynamics (Third Edition)*, J. Tu, G.-H. Yeoh, and C. Liu, Eds., Butterworth-Heinemann, 2018, pp. 125–154. doi: 10.1016/B978-0-08-101127-0.00004-0.
[30] Z. Ma, Q. Yang, and X. Su, “A Conforming augmented finite element method for modeling arbitrary cracking in solids,” *Journal of Applied Mechanics*, vol. 86, no. 071002, Apr. 2019, doi: 10.1115/1.4043184.
[31] C. Xu, Y. Long, and J. Wang, “Entrainment mechanism of turbulent synthetic jet flow,” *Journal of Fluid Mechanics*, vol. 958, p. A31, Mar. 2023, doi: 10.1017/jfm.2023.102.
[32] J. Feng, Y. Lin, G. Zhu, and X. Luo, “Effect of synthetic jet parameters on flow control of an aerofoil at high Reynolds number,” *Sādhanā*, vol. 44, no. 8, p. 190, Jul. 2019, doi: 10.1007/s12046-019-1173-2.
[33] K. C.S, “Study of flow field over fabricated airfoil models of NACA 23015 with its Kline-Fogleman variant,” 2013.